International Association
Bridge Earthquake Engineering

The Third International Bridge Seismic Workshop, 3rd IBSW
Seattle, Washington, USA - October 1st to 4th, 2019

EFFECTS OF PRESTRESSING ARRANGEMENTS ON SEISMIC FRAGILITY OF PRECAST SEGMENTAL BRIDGE COLUMNS

Yuye Zhang[(1),*], Mingxia Qin[(2)], Wei Hu[(3)]

[(1)]*Associate Professor, Department of Civil Engineering, Nanjing University of Science and Technology, Nanjing 210094, China, zyy@njust.edu.cn*
[(2)]*Graduate Student, Department of Civil Engineering, Nanjing University of Science and Technology, Nanjing 210094, China*
[(3)]*Engineer, Beijing Huawei Xinrong Construction Engineering Co., Ltd., Beijing 100097, China*

Abstract

Precast segmental bridge columns (PSBCs) are increasingly used in bridge structures for their numerous advantages compared with cast-in-place columns, such as the higher degree of assembly, shorter construction period, and better construction quality. However, the application of PSBCs in seismic region is limited due to their inferior seismic performance. To improve the seismic performance of PSBCs, this paper addresses the seismic fragility analysis of PSBCs with different layouts of prestressed tendons. Three-dimensional finite element (FE) models were developed to obtain the seismic capacity of the PSBCs with different prestressing arrangements. The FE models were verified by comparing the quasi-static analysis results with the previous test results. The analytical models of three-span continuous girder bridges with different PSBCs were established, and the seismic demand of the PSBCs was derived from the nonlinear time history analyses. Seismic fragility curves of the PSBCs were then constructed by comparing the seismic capacity and demand. The results indicate that the energy dissipation capacity of the PSBC with prestressed tendons at the center is greater than those of PSBCs with other prestressing arrangements, while the displacements of the column top of the former is relatively larger. The PSBCs with scattered prestressed tendons are less vulnerable to earthquakes when compared with those with centrally-placed prestressed tendons.

Keywords: precast bridge columns; prestressing arrangements; seismic performance; fragility analysis

1. Introduction

The prefabricated segmental bridge columns (PSBCs) possess the advantages of shorter construction period, higher construction quality and smaller impact on environment, compared with the monolithic bridge columns (MBCs) [1,2]. In recent years, PSBCs have been adopted in many bridge structures, such as Shanghai Yangtze River Bridge and Hong Kong-Zhuhai-Macao Bridge. It is generally believed that the bridge columns are important components in seismic design of bridge structures [3,4]. Thus, the evaluation of seismic performance for PSBCs has become a critical issue.

The damage indices of the bridge columns are necessary for establishing the vulnerability curves [5]. The damage indices of MBCs have been developed using various criteria, such as strength failure criterion, deformation failure criterion, energy failure criterion, deformation and energy double damage criterion [6-8]. Generally, the displacement ductility of MBCs are defined as the damage index, which is used for calculating the seismic demand and seismic capacity. Capacity limit states of MBCs can be described quantitatively by deformation failure criterion. But the damage mechanism of PSBCs is different from that of MBCs [1,9], which need to be further studied. The influence of prestressed tendons layout on the spatial stress characteristics of box girder bridges has been investigated by Xie et al. [10]. It was found that the interaction among prestresses in three directions was obvious. The optimization and reinforcement design of prestressed precast segmental bridges has been studied by Xu et al. [11]. However, little research exists on the seismic vulnerability of precast segmental bridge columns with different prestressing arrangements.

The objective of this paper was to evaluate the effects of prestressed tendon layouts on the seismic fragility of PSBCs. Firstly, the quasi-static analyses of PSBCs under cyclic loading were carried out to calculate the limit states of the PSBCs, corresponding to the seismic capacity. Nonlinear time-history analyses on the full bridge models, with different prestressed tendon layouts in PSBCs, were then conducted to obtain the seismic demands and damage indices of PSBCs. A suite of fifty recorded ground motions were applied to the bridge models. The vulnerability curves were finally developed by comparative analysis of the seismic capacities and demands of the PSBCs.

2. Analytical models

Three layouts of prestressed tendons (PTs) were designed to investigate the influence of their arrangement on the seismic capacity of PSBCs. As shown in Fig. 1, the column with centrally placed PTs was named as PSBC1. PSBC2 was arranged with two PTs at the section edge, and four PTs were arranged at the section edge in PSBC3. The PT spacing were both 160 mm in two horizontal directions. The calculated length of the column model was 1850 mm. Each column included 4 segments, and each segment had a diameter of 350 mm and height of 400 mm. Table 1 shows the design parameters of the three numerical test models.

Table 1 Design parameters of numerical test models

Specimen	Height of specimen (mm)	Diameter of specimen (mm)	Axial load rate	Number of PTs	Diameter of PTs (mm)	Layout of PTs
PSBC1	1850	350	0.224	1	22.0	Centrally-placed PTs
PSBC2	1850	350	0.224	2	15.6	Two scattered PTs
PSBC2	1850	350	0.224	4	11.0	Four scattered PTs

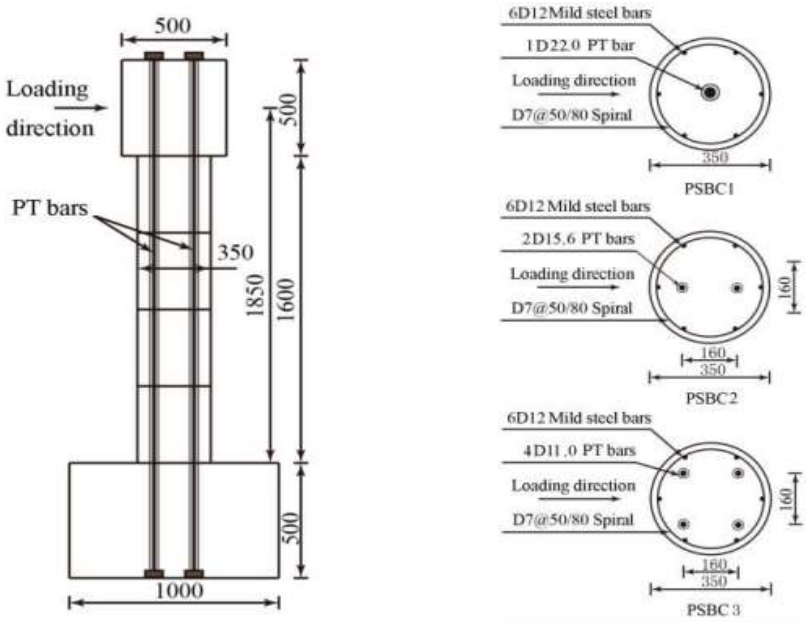

(a) (b)

Fig. 1. Columns with different PTs arrangments: (a) elevation layout, and (b) cross section (units: mm).

2.1 Model establishment

ABAQUS/Standard was adopted to develop the PSBC models correponding to the cyclic loading tests on PSBCs conducted by Bu et al. [12]. The finite element model is shown in Fig. 2. Column concrete was simulated by C3D8R element, and the Concrete Damage Plasticity model was selected to simulate column concrete behavior. Truss element (T3D2) was selected and embedded into concrete element to model the steel reinforcements. Beam element (B31) was used to simulate the unbonded PT tendons, which were designed to remain elastic throughout the test. PT force was exerted on the element using thermal method, by defining an expansion co-efficient for steel tendon material and predefined fields for temperature control in-between analysis steps, which can be calculated by following equations:

$$N = -\Delta T \alpha E A_s \tag{1}$$

$$\mu = N/(f_c A) \tag{2}$$

where ΔT is the temperature, N is the axial pressure, α is the expansion coefficient of prestressed tendons, E is the elastic modulus of prestressed tendons, A_s is the area of the prestressed tendon, μ is the axial compression ratio, and f_c is the axial stress of the concrete. A is the cross-sectional area. $\Delta T = -337.5℃$, $\alpha = 1.2 \times 10^{-5}$, $E = 2 \times 10^5 N/mm^2$, $A_S = 379.9mm^2$, $f_c = 14.3N/m^2$, $A = 96162.5mm^2$.

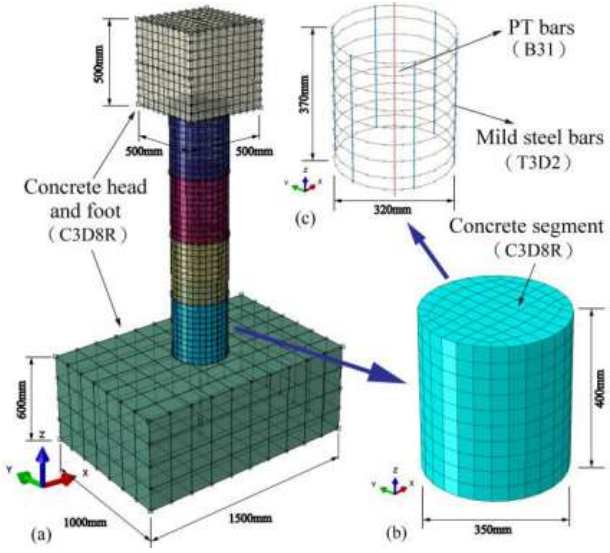

Fig. 2 Representative model of the PSBC

2.2. Model verification

The load-displacement (magnitude) hysteresis curve calculated by the PSBC model was compared with the experimental obtained from Reference [12]. As shown in Fig. 3, the numerical results are in good agreement with the experimental results, except those at the negative displacement stage. In the negative direction, the test lateral loads are slightly larger than the numerical results at larger drifts. This could due to the slip between the segments. The residual displacement occurred at the end of the positive unloading, so that the displacement in the negative direction is slightly larger than the positive direction [13]. In general, the numerical results agree well with the experimental results. The solid finite element model developed in this paper could be used to predict the energy dissipation capacity and residual displacement of the columns.

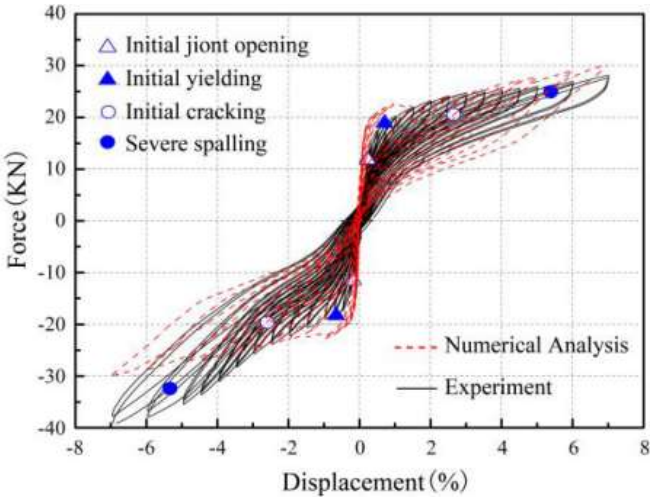

Fig. 3 Lateral force-drift curves derived from the numermal analyses and tests [12]

3. Vulnerability analysis

3.1. Analytical mothod

To estimate the damage probability of PSBCs during a seismic event, the vulnerability analysis method was adopted in this study. The vulnerability function represents the probability of the seismic demand of the column exceeding the seismic capacity under seismic excitations with specific intensities. The seismic demand value (S_d) can be obtained through nonlinear time-history analysis of the bridge model under an ensemble of ground motion records, which can be represented by an appropriate intensity measure (IM). The peak ground acceleration (PGA) is selected as the IM in this paper. The seismic capacity value (S_c) can be obtained through quasi-static analysis of the PSBC model. Since S_d and S_c both follow the lognormal distribution, the vulnerability function can be expressed as

$$P_f[S_d \geq S_c|IM] = \Phi\left[\frac{lnS_d - lnS_c}{\sqrt{\beta_d{}^2 - \beta_c{}^2}}\right] = \Phi\left[\frac{a + blnPGA - lnS_c}{\sqrt{\beta_d{}^2 - \beta_c{}^2}}\right] \quad (3)$$

where S_d is the structural demand, S_c is the stuctural capacity, β_d is Standard deviation of the lognormal distribution of seismic demand, β_c is Standard deviation of the lognormal distribution of seismic capacity, $\Phi(.)$ is the standard normal cumulative distribution function, *a* and *b* are regression coefficients based on the S_d and *IM* from the nonlinear time-history analysis for the bridge model and analysis of the selected ground motion, respectively.

3.2. Damage index formula

As mentioned above, limit states of MBC can be described quantitatively with deformation formula. In this paper, the damage index formula of maximum deformation and cumulative hysteretic energy consumption proposed by Park-Ang was used to define limit states of PSBCs [14], as expressing in following equation:

$$DI = \frac{\delta_{max}}{\delta_u} + \frac{\beta}{Q_y + \delta_u}\int dE \quad (4)$$

where δ_{max} is the maximum displacement when the state of failure is reached, which can be obtained from the hysteresis curve. δ_u is ultimate deformation of the column, taking Pushover analysis results. Q_y is the yield strength of the column, taking the lateral loading force when the strain of the prestressed tendon

reaches the yield strain. $\int dE$ is accumulated hysteretic energy of columns when the state of failure is reached, and β is Correction factor, which can be reversed according to *DI*=1 when collapse occur [14].

Hwang et al. [7] modified the Park-Ang formula and proposed the relationship between damage state and damage index The Park-Ang damage index model was employed to obtain the relationship between the damage index and the lateral displacement amplitude of the unbonded prestressed assemble column [15]. However, quantitative limit states on seismic capacity of PSBCs are rarely studied. In the next part, lateral force-drift curves combined with energy dissipation curve and capacity parameters monitored in cyclic loading quasi-static analysis will be studied, then DI of PSBCs will be captured.

3.3. Seismic capacity

The limit states are indications of the capacity to sustain different levels of the engineering demand parameters chosen, and are quantitative, indicating the realization of the damage state. Based on the Park-Ang's damage model, qualitative limit states must be derived for the bridge of interest. These limit states should be defined in consistent parameters such as the capacity parameters monitored in cyclic loading quasi-static analysis [16]. For MBC, column damage is measured in terms of the column displacement ductility ratio [17]. Regarding column ductility displacement limit states, Tavares et al. [16] conducted a study specifically for the Chemin des Dalles bridge columns, with a sectional analysis program and a damage mechanics-based program [18]. Three types of quantitative limit states were defined for the bridge columns, drift, curvature ductility, and displacement ductility. This paper combined the displacement ductility ratio, the concrete compressive strain and the prestressed tendon tensile strain monitored in the quasi-static cyclic loading test and residual displacement to jointly define the limit state of the column.

After the relevant data are sorted, the four limit states of PSBC are quantitatively described, as shown in Table 2. Limit 1 can be defined as the displacement ductility reaches 1.0 or the compressive strain of the cover concrete reaches 0.002. Limit 2 can be defined as the displacement ductility reaches 1.2 or the compressive strain of the core concrete reaches 0.012. Limit 3 can be defined as the displacement ductility reaches 1.76 or the compressive strain of the core concrete reaches 0.018 or the PT strain reaches 0.007. Limit 4 can be defined as the displacement ductility reaches 4.76 or the compressive strain of the core concrete reaches 0.02 or the residual drift reaches 0.8%l_b.

Table 2 Minimum limit corresponding to damage states of the PSBC

Damage states	Displacement Ductility (Hwang et al. 2000)	Compressive Strain	PT Strain	Residual Drift
Slight damage	1.0	0.002 (cover concrete) (Bu et al. 2016)	NA	NA
Moderate damage	1.2	0.012 (core concrete) (JTG/T B02-01-2008)	NA	NA
Severe damage	1.76	0.018 (core concrete)	0.007 (Wing et al. 2003)	NA
Collapse	4.76	0.02 (core concrete)	NA	0.8%l_b (Wing et al. 2003)

Note: l_b is the effective height of the column.

According to the above modeling process and the minimun limit in Table 2, lateral force-drift curves of PSBC1, PSBC2 and PSBC3 were developed, the maximum displacement amplitude δ_{max} corresponding to each damage state was marked in the hysteresis curves as shown in Fig. 4. When the horizontal loading force is reduced to 0, the tops of the three columns can return to the initial position relatively well, and the residual displacement is small. PSBC is with good self-resetting ability. For PSBC1, slight damage, moderate damage, severe damage and collapse occured when displacement amplitude reached 2%, 3.5%, 4.5% and 6% respectively. For PSBC2, limit 1 to 4 occured when displacement amplitude reached 2.5%, 3.5%, 5% and 7%, limit 1 to 4 of PSBC3 occured when displacement amplitude reached 2.5%, 4.0%, 5% and 7%.

Fig. 5 shows the energy dissipation curves of the three column models. It can be seen that PSBC1 exhibits the best energy dissipation capacity in the three PSBCs. The cumulative energy consumption is 757.7 kN (the unit of displacement is taken as 1), and the energy dissipation of PSBC2 and PSBC3 are 637.8 kN and 636.5 kN, respectively. The energy consumption of PSBC2 and PSBC3 are 15.8% and 16.0% smaller than that of PSBC1, respectively.

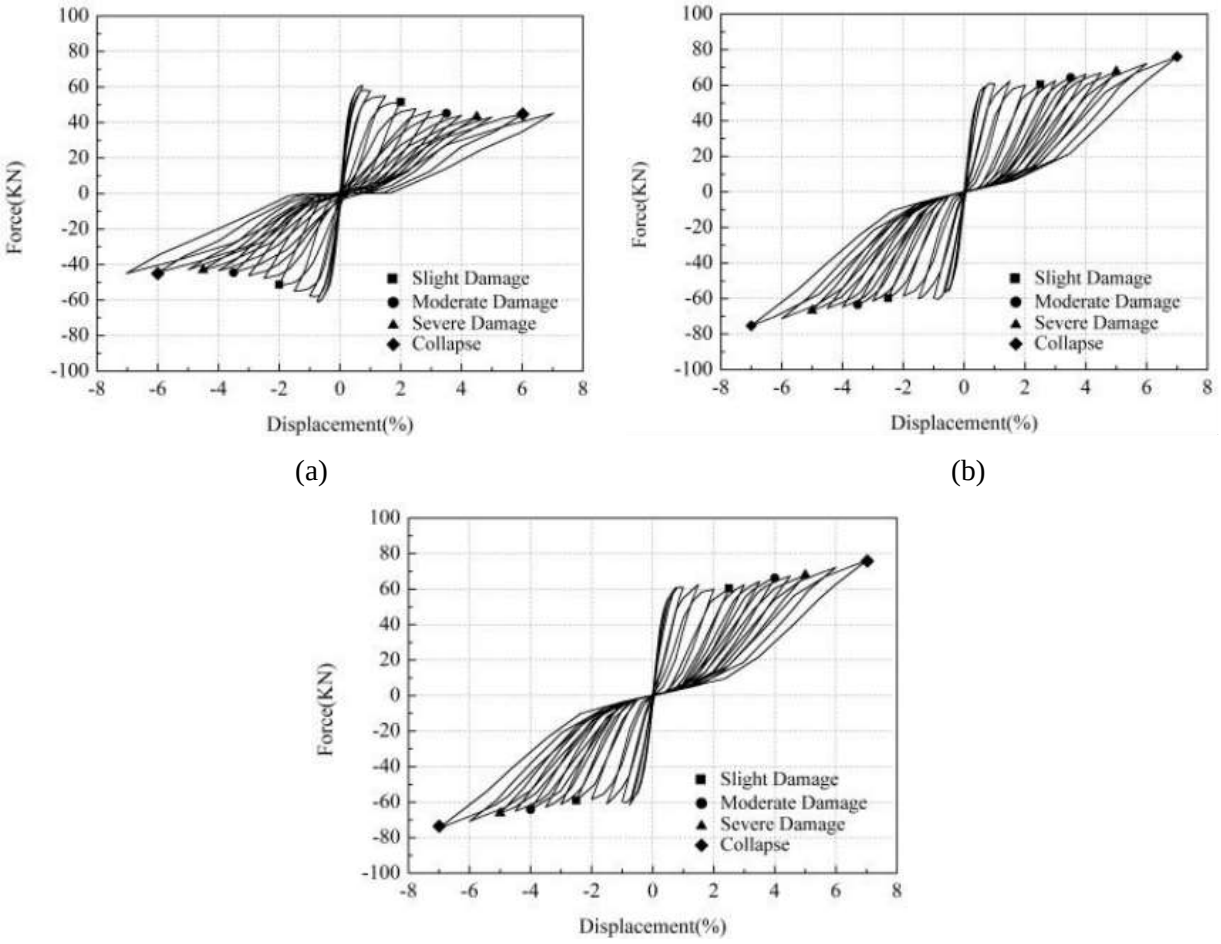

Fig. 4 Lateral force-drift curves: (a) PSBC1; (b) PSBC2; and (c) PSBC3

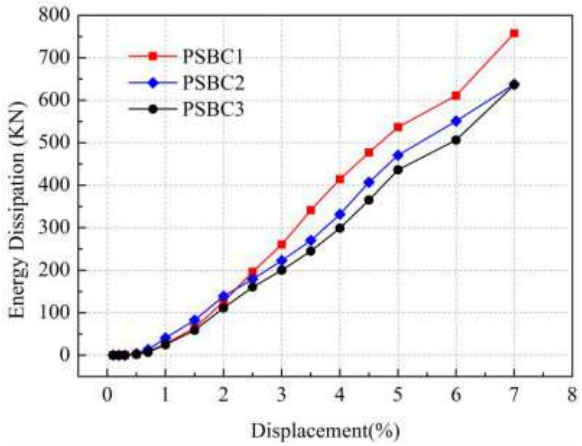

Fig. 5 Energy dissipation curves

According to the damage index formula proposed by Park-Ang, expressed as Equation (4), the damage parameters of the three columns were calculated. Table 3 lists the main parameters for calculating the damage indices of the PSBCs. Based on the parameter values in the Table 3, the limit-state capacities at four damage states of the three PSBCs were derived, as listed in Table 4.

Table 3 The main parameters for calculating the damage indices of the PSBCs

Specimen	δ_u (%)	Q_y (KN)	β (10^{-4})	Slight damage		Moderate damage		Severe damage		Collapse	
				δ_{max} (%)	$\int dE$ (KN)	δ_{max} (%)	$\int dE$ (KN)	δ_{max} (%)	$\int dE$ (KN)	δ_{max} (%)	$\int dE$ (KN)
PSBC1	8	51.3	16.80	2.0	126.00	3.5	341.69	4.5	477.15	6.0	611.20
PSBC2	8	60.4	9.47	2.5	179.15	3.5	270.28	5.0	470.69	7.0	637.8
PSBC3	8	62.8	9.87	2.5	160.47	4.0	299.02	5.0	436.44	7.0	636.51

Table 4 Limit-state capacities of PSBCs

Damage states	*DI*		
	PSBC1	PSBC2	PSBC3
Slight damage	0.302	0.348	0.344
Moderate damage	0.570	0.490	0.559
Severe damage	0.758	0.717	0.711
Collapse	1.0	1.0	1.0

3.4. Seismic demand

In order to obtain the seismic response of the PSBCs of bridge structures under ground motions, three-span continuous girder bridge models were constructed by SAP2000. Nonlinear time history analyses of the bridges under 50 ground motions were carried out. The columns adopted three forms of PSBCs as illustrated in Fig. 1 in Section 2. The bridge had three spans, which are 22.0 + 30.0 + 22.0 m. Fig. 6 shows the bridge elevation. The sliding bearings were arranged between the girders and the columns, or between the girders and the abutments. The abutment was fixed to the ground, as conducted in [19]. Two bearings were placed on each column, and there were four bearings on each abutment.

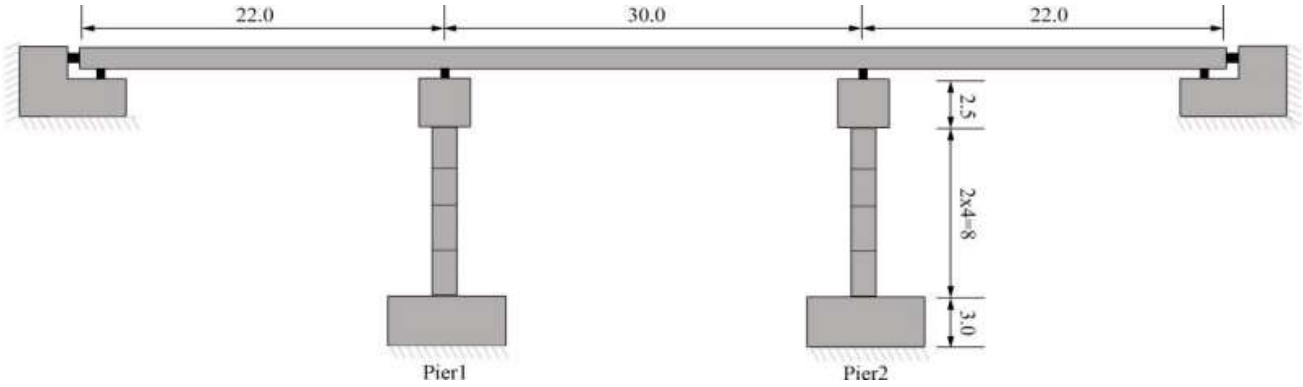

Fig. 6 Bridge elevation (units: m)

A key factor in the analysis of vulnerability is the uncertainty of seismic intensity measure. The PGA is taken as the intensity measure in this paper. A suit of 50 seismic waves were selected from the PEER Ground Motion Database (http://peer.berkeley.edu/smcat). The acceleration time-history curves of these seismic waves are shown in Fig. 7. The 50 seismic waves are input into three full-bridge models respectively for seismic demand analyses.

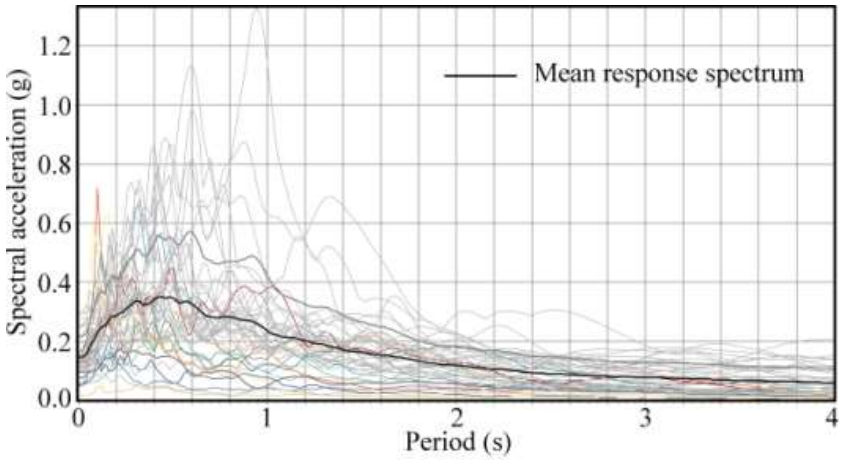

Fig. 7 Response spectra for the selected ground motions

Based on the nonlinear time-history analyses of the full-bridge models, the displacement amplitudes of the PSBCs under ground motions were obtained. Table 5 lists the displacement distribution of PSBCs. It is indicated that the displacement of PSBC1 is mainly concentrated between 3% and 4%, while the displacement of PSBC2 and PSBC3 are mainly between 2% and 3%. It can be seen that the seismic response of the PSBCs with scattered PTs is smaller than that of the centrally-placed PTs. According to the displacement and energy consumption curve, the energy consumption of the columns corresponding to each seismic wave can be obtained. The energy consumption was taken into Equation (4) to obtain the seismic demand (S_d) of the PSBCs under 50 seismic waves. Table 6 lists the S_d distribution of the PSBCs. It shows that the seismic damage of the columns with scattered prestressing tendons is generally smaller than that of the columns with central PTs. Regression analyses were conducted for the logarithm of PGA and S_d, and the linear relationship between lnS_d and lnPGA was then obtained, as shown in Fig. 8.

Table 5 Displacement distribution of PSBCs

Displacement (%)	PSBC1	PSBC2	PSBC3
(0, 1]	0	2	2
(1, 2]	5	6	6
(2, 3]	7	19	19
(3, 4]	21	11	11
(4, 5]	7	5	5
(5, 6]	2	4	4
(6, 7]	2	2	2
(7,+∞)	6	1	1

Table 6 S_d distribution of PSBCs

S_d	PSBC1	PSBC2	PSBC3
(0, 0.2]	1	4	4
(0.2, 0.4]	8	21	22
(0.4, 0.6]	14	14	13
(0.6, 0.8]	13	6	6
(0.8, 1.0]	6	3	3
(1.0,+∞)	8	2	2

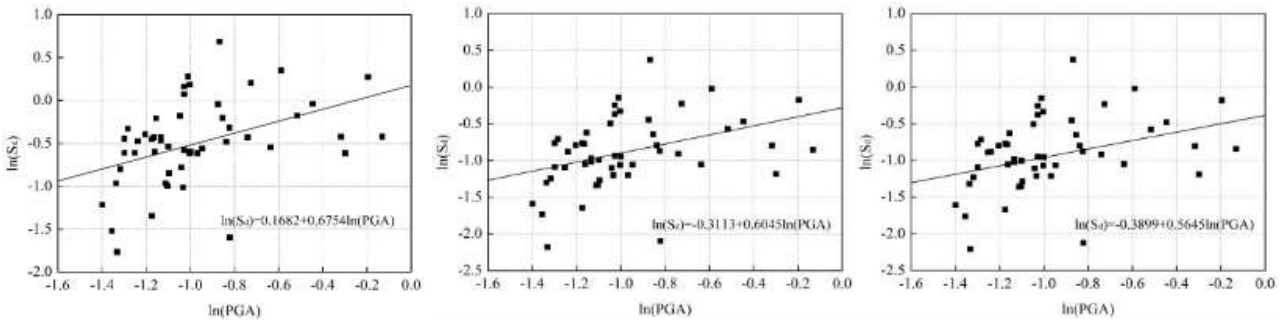

(a) (b) (c)

Fig. 8 Probabilistic seismic demand models of PSBCs: (a) PSBC1; (b) PSBC2; and (c) PSBC3

4. Fragility curves

Fig. 9 shows the fragility curves of PSBCs at different damage states. It can be seen from Fig. 9 that the probabilities for reaching each damage states of the column increases with the increase of PGA, and the probabilities at slight damage is the most obvious. Under the same PGA, The more severe the damage to the pier, the smaller the probabilities of occurrence. For PSBC1, the probabilities of slight damage are close to 100% when PGA is greater than 60%, the maximum probabilities of occurrence of moderate and severe damage are both over 80%, and the maximum probability of collapse excedes 60%. For PSBC2, the maximum probabilities, at slight, moderate, severe, and collapse damage states, are 93.1%, 78.9%, 51.7%, and 26.7% respectively, which was significantly lower than PSBC1. The probability of occurrence of four damage states in PSBC3 is lower than PSBC2, which are 91.2%, 64.9%, 46.1%, and 21.8%, respectively.

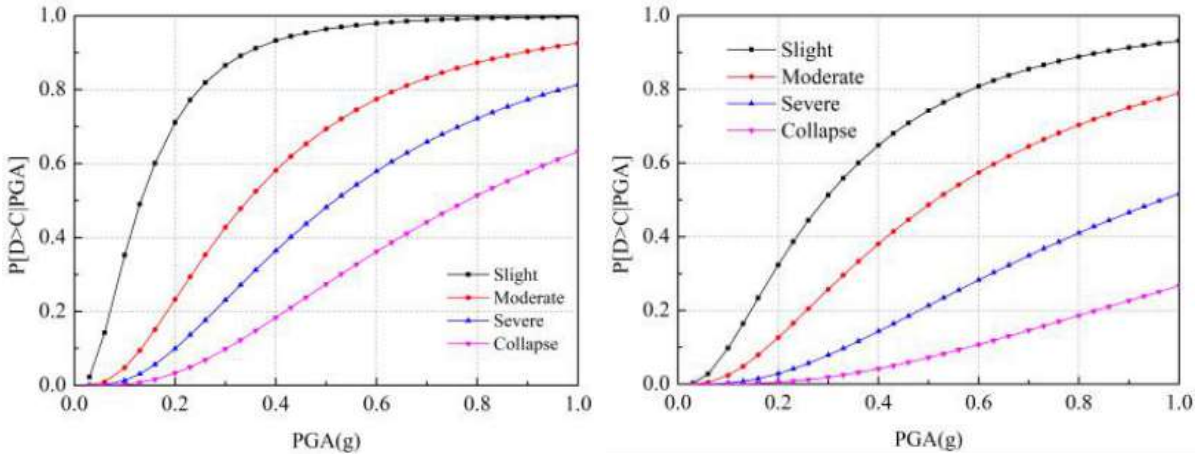

(a) (b)

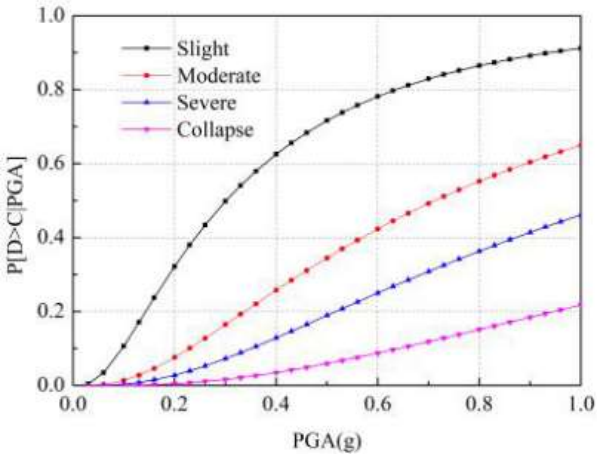

(c)

Fig. 9 Fragility curves of PSBCs at different damage states: (a) PSBC1; (b) PSBC2; and (c) PSBC3

Fig. 10 compares the fragility curves of the different PSBCs for each damage state. It is illustrated that the damage probability of PSBC1 are greater than those of PSBC2 and PSBC3 at slight damage state, when the PGA is 0.6 g. The maximum probability of PSBC1 at slight damage state reaches 97.9%, while those of the other two columns are about 80%. The differences in the probabilities of the three columns are obvious at moderate damage state. At moderate damage state, PSBC1 has the largest damage probabilities, followed by PSBC2, and PSBC3. For the severe and collapse damage states, the damage probabilities of PSBC2 and PSBC3 are relatively close, while the damage probabilities of PSBC1 are much greater than those of PSBC2 and PSBC3.

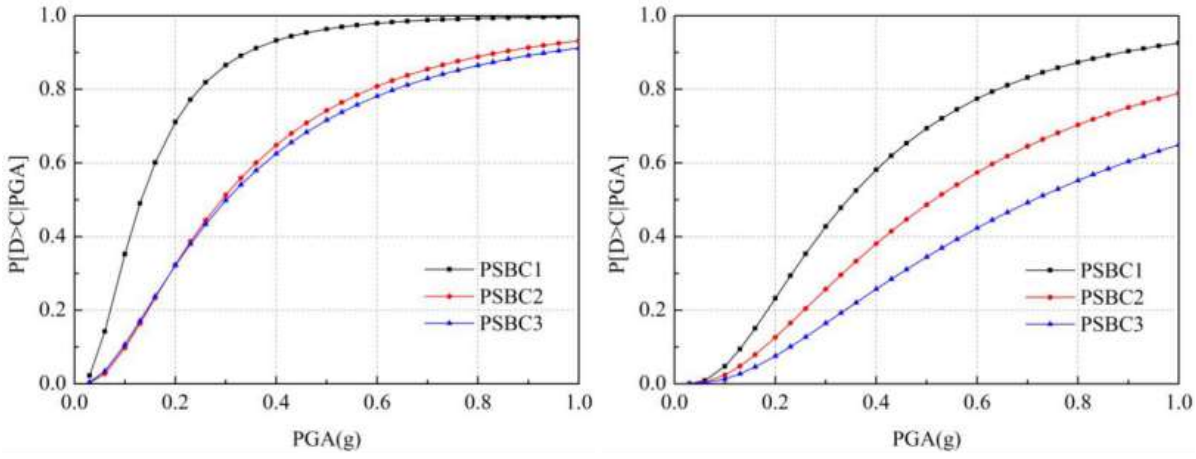

(a) (b)

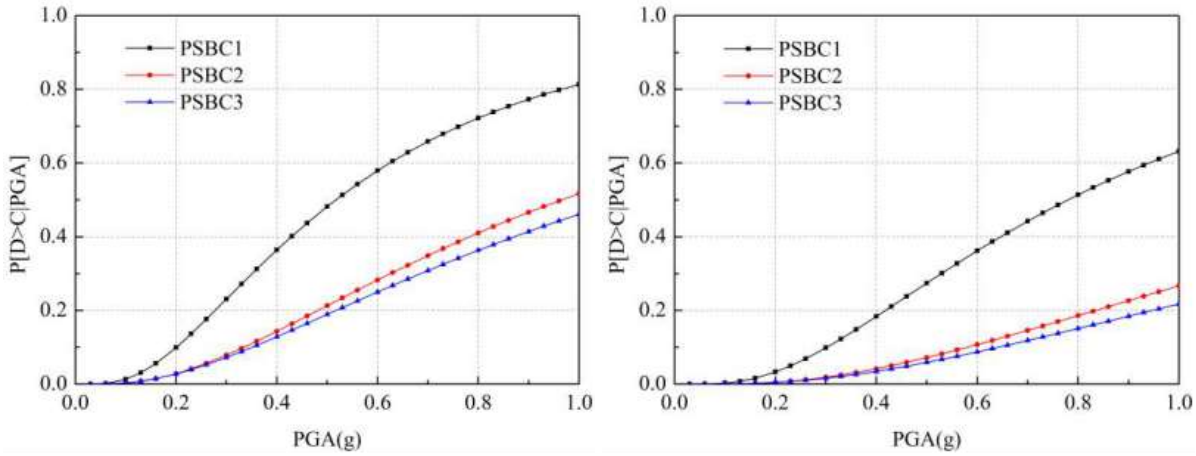

(c) (d)

Fig. 10 Comparison of fragility curves of different PSBCs for each damage state: (a) slight damage; (b) moderate damage; (c) severe damgae; and (d) collapes

5. Conclusions

This study investigated the effects of the prestressing arrangement of on the seismic fragility of PSBCs. Three-dimensional finite element models of PSBCs with three different prestressed tendon layouts were developed, and the quasi-static analyses of the PSBCs were carried out to obtain their damage indexes. Nonlinear time-history analysis on the full-bridge models with different PSBCs were conducted. The seismic demand of the PSBCs of the bridges was derived. Finally, the seismic vulnerability curves of the PSBCs with the prestressed tendon arrangements were constructed and analyzed. Following conclusions can be drawn:

(1) The PSBC with centrally-placed prestressed tendons has larger energy dissipation capacity, compared with those with scattered prestressed tondons, while the displacements of the former are relatively greater under ground motions.

(2) The seismic fragilty of the PSBC, with centrally-placed prestressed tendons, is greater than that of the PSBCs with scattered prestressed tondons at four damage states. This indicates that the PSBCs with scattered prestressed tondons tend to be less vulnerable under earthquakes.

(3) The damage exceeding probabilities of the PSBC with two scattered prestressed tendons are significantly larger than that of the PSBC with four scattered prestressed tendons, at moderate damage state. However, the probabilities are close for the two PSBCs at other damage states.

6. Acknowledgements

This study was supported by the National Natural Science Foundation of China (Grant No. 51508276), and the China Scholarship Council (Grant No. 201806845051).

5. References

[1] Zhang Y, Fan W, Zhai Y, Yuan W (2019): Experimental and numerical investigations on seismic behavior of prefabricated bridge columns with UHPFRC bottom segments. *Journal of Bridge Engineering*, **24** (8), 04019076.

[2] Ge JP, Yan XF, Wang ZQ (2017): Seismic performance analysis of tail transit segmental bridge columns with mechanical splices. *Earthquake Engineering and Engineering Dynamics*, **37** (6), 143-153.

[3] Yang CS, DesRoches R, Padgett JE (2009): Vulnerability curves for a typical california box girder bridge. *Technical Council on Lifeline Earthquake Engineering Conference 2009*, Oakland, USA.

[4] Zhang Y, Zhai Y (2018): Improvements in seismic performance of prefabricated bridge piers. *Journal of Highway and Transportation Research and Development*, **12** (2), 43-50.

[5] Zhai Y, Zhang Y (2018): Damage index analysis of prefabricated segmental bridge columns under cyclic loading. *Latin American Journal of Solids and Structures*, **15** (11), e137.

[6] Diaz SA, Pujades LG, Barbat AH, Vargas YF, Hidalgo-Leiva DA (2017): Energy damage index based on capacity and response spectra. *Engineering Structures*, **152**, 424-436.

[7] Hwang H, Jernigan JB, Lin YW (2000): Evaluation of seismic damage to Memphis bridges and highway systems. *Journal of Bridge Engineering*, **5** (4), 322-330.

[8] Ibarra LF, Medina RA, Krawinkler H (2005): Hysteretic models that incorporate strength and stiffness deterioration. *Earthquake Engineering and Structural Dynamics*, **34**, 1489-1511.

[9] Solberg K, Mashiko N, Mander JB, Dhakal RP (2009): Performance of a damage protected highway bridge pier subjected to bidirectional earthquake attack. *Journal of Structural Engineering*, **135** (5), 469-478.

[10] Xie J, Zhang JQ, Zheng XH (2011): Prestress tendons layout considering spatial stress characteristics of prestressed concrete box-girder bridges. *11th International Conference of Chinese Transportation Professionals (ICCTP)*, Nanjing, China.

[11] Xu D, Lei J, Zhao Y (2016): Prestressing optimization and local reinforcement design for a mixed externally and internally prestressed precast segmental bridge. *Journal of Bridge Engineering.* **21** (7), 05016003.

[12] Bu ZY, Ou YC, Song JW, and Zhang NS (2016): Cyclic loading test of unbonded and bonded posttensioned precast segmental bridge columns with circular section. *Journal of Bridge Engineering*, **21** (2), 04015043.

[13] Qin M, Zhang Y, Zhai Y, Yuan W (2018): Influence of prestressed strands layout on seismic behavior of segmental bridge piers. *Earthquake Engineering and Engineering Dynamics*, **38** (4), 158-163.

[14] Park YJ, Ang AH (1985): Mechanistic seismic damage model for reinforced concrete. *Journal of Structural Engineering*, **111** (4), 722-739.

[15] Bu ZY, Wu WY (2015): Experiment on seismic behavior of precast segmental concrete bridge columns under quasi static cyclic loading. *Journal of Architecture and Civil Engineering*, **32** (1), 42-50.

[16] Tavares DH, Suescun JR, Paultre P, Padgett JE (2013): Seismic vulnerability of a highway bridge in Quebec. *Journal of Bridge Engineering*, **18** (11), 1131-1139.

[17] Hwang H, Liu JB, Chiu YH (2001): Seismic fragility analysis of highway bridge. Mid-America Earthquake (MAE) Center, Technical Report, MAEC Report 01-06.

[18] LaBorderie C (1991): Unilateral phenomena in damageable material: modeling and application to the analysis of concrete structure. PhD Thesis, University of Paris, Paris, France.

[19] Zhang Y, Xiao F, Badar J (2019) Influence of straining beams on the seismic fragility of double-column bridge piers. *The Civil Engineering Journal*, **1**, 32-44.